American Journal of Applied Sciences

Article

Crosslinked Facilitated Transport Membranes Based on Carboxymethylated NFC and Amine-Based Fixed Carriers for Carbon Capture, Utilization, and Storage Applications

Benjamin Dhuiège [1,*], Elsa Lasseuguette [2], Marie-Christine Brochier-Salon [3], Maria-Chiara Ferrari [2] and Karim Missoum [1]

[1] InoFib, 461 rue de la Papeterie, CEDEX, CS10065 F-38402 St-Martin-d'Hères, France
[2] School of Engineering, University of Edinburgh, Robert Stevenson Road, Edinburgh EH9 3FB, UK
[3] University Grenoble Alpes, CNRS, Grenoble INP, LGP2, F-38000 Grenoble, France

Abstract: Herein, we report the performances of crosslinked facilitated transport membranes based on carboxymethylated nanofibrils of cellulose (cmNFC) and polyvinylamine (PVAm) with the use of 3-(2-Aminoethylamino) propyltrimethoxysilane (AEAPTMS) as second fixed carrier for CO_2 selectivity and permeability. The grafting of AEAPTMS on cmNFC was optimized by following the hydrolysis/condensation kinetics by ^{29}Si Nuclear Magnetic Resonance (NMR) analyses and two different strategies of the process of membrane production were investigated. In optimized conditions, around 25% of the -COOH functions from cmNFC have crosslinked with PVAm. The crosslinked membranes were less sensitive to liquid water and the crystallinity of PVAm was tuned by the conditions of the membrane elaboration. In both processes, CO_2 selectivity and permeability were enhanced especially at high water vapor concentration by the use of PVAm and AEAPTMS suggesting the existence of a facilitation effect due to amine-CO_2 interaction, while the mechanical integrity of the swollen membranes remained intact.

Keywords: amine-based fixed site carrier crosslinked facilitated transport membranes; carboxymethylated nanofibrils of cellulose; carbon capture utilization and storage

1. Introduction

Over the last few decades, one of the major environmental challenges has been reducing emissions of greenhouse gases to the atmosphere—especially carbon dioxide (CO_2)—and minimizing the carbon footprint due to anthropogenic activities [1]. In the foreseeable future, industries will need to comply with increasingly strict regulations on CO_2 emissions. Thus, carbon capture, utilization, and storage (CCUS) technologies appear to be a viable industrial low-cost alternative to prevent its dispersion in the environment towards a zero-emission pathway for energy production [2,3].

Several technologies have been proposed to capture CO_2 from power plant emissions, including absorption, adsorption, cryogenic distillation, and membrane separation [2].

Traditionally, for post-combustion processes, packed columns have been used for absorption but this technique is energy consuming and suffers from various problems including flooding, foaming, and/or solvent degradation [4]. Membrane separation presents many advantages, like compactness, and easy integration in already installed facilities [2–9].

In the current commercial gas separation membranes, mainly based on dense polymer, the transport can be described by a solution-diffusion mechanism, depending on the kinetic diameter and condensability of the gas molecules [10]. This mechanism, however, tends to suffer from an inherent trade-off between permeability and selectivity, which limits the separation performance of the materials [11,12]. A number of strategies has been developed over the years to overcome this limitation, using, for example, mixed matrix membranes [13–15] or polymer and block copolymers with high CO_2 affinity [16–19]. As an alternative to conventional polymeric membranes, facilitated transport membranes (FTMs) have attracted attention because of the potential to achieve both high permeability and high selectivity [20,21]. FTMs selectively permeate CO_2 by adding to the transport of free CO_2 molecules an additional mechanism of facilitated diffusion through complexation with an agent incorporated in the membrane, named carrier [22–25], whereas gases such as H_2, N_2, and CH_4 will permeate exclusively by a solution–diffusion mechanism. For CO_2 separation, amine moieties represent a quite reasonable choice as carriers which was exploited in several works [26–30]. The mechanism, which regulates the interaction between aminated molecules and CO_2, is not yet completely understood, even though two main reactions are commonly considered to occur within the matrix [30–32]. When unhindered amines are present, carbon dioxide tends to form a carbamate ion through a zwitterion mechanism, a pathway originally described by Caplow [33] and presented in Figure 1a. If a hindered amine is present, a second mechanism is preferred, due to the carbamate ion instability, related to its large steric hindrance as presented in Figure 1b [30].

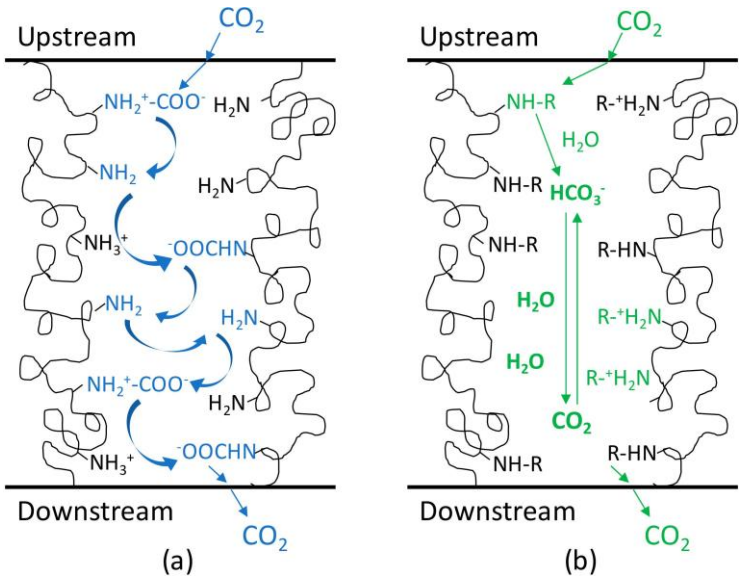

Figure 1. Preferential pathways and mechanisms of CO_2 molecules through unhindered (**a**) or hindered (**b**) amines groups across the membranes.

In both schemes, the reaction starts at the upstream side of the film, which represents the complexing of CO_2 to the carrier molecule once the gas is dissolved. The opposite reaction will take place at the downstream side, leading to the decomplexation of the carbon dioxide and allowing the molecule to pass once again into the gaseous phase.

Historically, the earliest examples of FTMs were supported liquid membranes (SLM), introduced by Ward and Robb [23]; they impregnated the pores of a microporous support with a carrier solution enabling the CO_2 molecules to bond with functional group capable of permeating through the film and

releasing them on the downstream side. With this system, they managed to achieve excellent separation performances. For instance, selectivity of 1500 was reported for CO_2/O_2 [23,34]. Despite high selectivity and permeability performances, these membranes lacked severely in terms of stability, mainly because of carrier leakages and deactivation due to evaporation or entrainment with the gas stream [35].

To tackle this instability issue, recent research has been focused on fixed site carrier (FSC) membranes. These membranes have functional carriers that are covalently bonded to the matrix polymer backbone or to a dispersed secondary phase restricting their mobility but drastically improving the membrane stability [21,31,36]. Both approaches showed strengths and weaknesses: small mobile carriers tend to leak and evaporate, while fixed carriers can struggle to achieve the same diffusion rates due to their lack of mobility. However, the diffusivity of a swollen FSC membrane should display performances between that of a mobile and a fixed carrier.

Among the numerous amine-based FTMs used for CO_2 separation and extensively investigated in last decades [20,21,37–42], polyvinylamine (PVAm) is an attractive aminated common polymer to prepare FSC membranes [29]. Thanks to its hydrophilicity and high amount of amine moieties, PVAm presented good separation performances in various conditions [43–45]. In presence of water, these amine groups are able to interact with CO_2 [31]. Moreover, as presented in the mechanisms above, the amine groups can also play the role of catalyst in the CO_2 hydration reaction [46]. However, PVAm can also suffer from instability issues, due to the poor mechanical properties achieved at high humidity [47].

This problem is usually overcome by blending PVAm with a 'structural' polymer, which can increase the mechanical properties of the matrix under high humidity conditions, still allowing the facilitated transport mechanism. In several works, PVAm has been blended with different materials such as (i) polyvinyl alcohol (PVA) [48–50], (ii) carbon nanotubes [44,46,49,51], and (iii) native nanofibrillated cellulose (NFC) [52,53], showing positive results in term of stability and separation performance. Other approaches to obtain more stable materials can rely on the use of a high molecular weight PVAm, as proposed by Chen and Ho [54].

In this work, carboxymethylated nanofibrillated cellulose (cmNFC) was chosen as a 'structural' polymer. Actually, for sustainability and green technology development, it appears essential to prepare new membranes for carbon capture using bio-based materials such as cmNFC. Cellulose is the most abundant biopolymer on earth. Extracted most often from wood or annual plants, cellulose fibers are composed of several fibrils which were firstly isolated by Turbak et al. [55] in 1983 and are usually used as microfibrillated cellulose (MFC), cellulose nanofibrils (CNF), or nanofibrillated cellulose (NFC) obtained after mechanical disintegration. Since 2008, the development of NFC, which represents one of the most studied bio-based materials [56–59], attracts exponential interest from researchers, as well as industrial companies, with more than 60 producers worldwide. More recently, in 2016, NFC was identified as the second bio-economy priority in Europe thanks to its properties. Indeed, NFC displays high mechanical resistance and excellent barrier properties, and it is also biodegradable and biocompatible, highlighting this bio-based material as an excellent candidate in several applications such as packaging [58], paper and board [60], composites [61], printed electronics [62], biomedical devices [63], etc. Also, in the field of membranes, nanocellulose is gaining attention; in the last three years, several papers appeared using this material as a base for the production of gas separation membranes [52,53,64–66]. To isolate NFC from fibers, an enzymatic or chemical pretreatment is performed in order to weaken cellulosic fibers interactions, as well as to reduce the energy consumption of the production process during the mechanical step [67–70]. The fibers have diameters within the nanometric scale and lengths in the order of few micrometers [58,59], thus resulting in a very high aspect ratio, and can show an individual tensile modulus up to 100 GPa [71]. In several works, this material has been successfully employed as a reinforcing agent for polymeric structures [71,72], especially due to its ability to achieve the percolation threshold already at few percent of loading, when opportunely dispersed in a matrix [59,72]. As already mentioned, a previous work [52] investigated the gas transport properties of different type of NFC pure and in a 50/50

wt % blend with PVAm, showing that the resulting film has very interesting separation performances (CO_2/N_2 larger than 400 and CO_2/CH_4 larger than 350) at an intermediate relative humidity. At higher humidity, though, the material showed a strong decrement of the separation performances, most likely due to excessive water sorption, which caused a severe loss of mechanical integrity. To tackle this issue, one of the solutions is to functionalize the cellulosic fibers with a carboxymethylation process [73,74]. This modification was already reported in numerous papers with specific properties attributed to carboxymethylated NFC, i.e., highly charged surface (which can lead to ionic interactions with other molecules), and more acid groups at the surface (for post-modification purpose) in comparison to neat NFC [75,76]. Thanks to their many carboxylic functions on the surface, cmNFC fibers are able to be easily crosslinked with several amino compounds. For instance, at high temperatures they can be crosslinked with the amine functions of PVAm forming amide bonds [77], which improves the mechanical strength of the swollen PVAm membrane at high humidity, and thus, should enhance the gas transport properties of CO_2 through the swollen membranes with increasing water content present in the gas stream.

To further improve the compatibility between PVAm and cmNFC, aminosilanes can be used [78,79], such as 3-(2-Aminoethylamino) propyltrimethoxysilane (AEAPTMS). In this work, this aminosilane will be grafted on the cellulosic material by the reaction between the remaining hydroxyl moieties of cmNFC and the alkoxysilanes groups through silylation after hydrolysis/condensation reactions [78]. Beside, AEAPTMS bears two amine groups, one hindered and one unhindered, which can participate in the two pathway mechanisms presented in Figure 1, and thus, can enhance the CO_2 selectivity and permeability through the membrane in addition.

In the current report, new bio based materials for CO_2 separation have been developed, based on cmNFC-PVAm crosslinked membranes with the presence of an aminosilane as a second fixed carrier to enhance the CO_2 permeability compared to the use of neat NFC [52,65,79], amino acids [64] or other type of aminosilane [79] in literature. The grafting of aminosilane has been optimized by following the hydrolysis/condensation reactions by ^{29}Si NMR analyses. Different strategies have been employed to produce performant and water-swellable crosslinked membranes. While Fourier-Transform InfraRed (FTIR) spectroscopy was used in order to observe the covalent bonds between amine and carboxylic functions, Differential Scanning Calorimetry (DSC) analyses were carried out to confirm the crosslinking and determine the thermal characteristics of the membranes. Mechanical tests were also performed to assess the mechanical strength of the membranes and then, water uptake were investigated to identify their swelling properties in presence of liquid water. Air permeability and surface hydrophilicity were also studied. The morphology and the composition of the novel biobased membranes were examined using field emission gun (FEG-SEM), energy-dispersive X-ray (EDX), and elemental analyses techniques. Finally, CO_2 and N_2 permeability measurements were carried out on the facilitated transport membranes at 40 °C and 75% and 95% of relative humidity.

This overall combination represents an interesting approach to facilitate gas separation in membranes and the use of sustainable cellulosic materials. To the best of our knowledge, there are very few papers and amine-based functional groups in carbon capture membranes, mainly dealing with cmNFC–aminated polymers blends [52,64,65] or with NFC grafted with aminosilanes [79].

2. Materials and Methods

2.1. Materials

Cellulose pulp was originated from soft wood provided by Fibre Excellence Saint-Gaudens. Highly pure sodium hydroxide (NaOH) was bought from Fisher Scientific. Sodium hydrogenocarbonate 99% ($NaHCO_3$), sodium chloroacetate 98% ($ClCH_2COONa$), 3-(2-Aminoethylamino) propyltrimethoxysilane 96% (AEAPTMS) were purchased from Alfa Aesar, acetic acid (CH_3COOH) from Carlo Erba and both ethanol 96% and isopropanol 99% from Revol. The products were not further purified before their use. Lupamin 9095 was provided by BASF and

dialyzed in a 1 kDa cut-off bag for 7 days in distilled water bath replaced two times per day to remove the sodium formate salt from the commercial product and obtain a purified aqueous solution of poly(vinyl amine) (PVAm).

2.2. Preparation of Carboxymethylated NFC

Carboxymethylated nanofibrils of cellulose (cmNFC) were prepared following two main steps. First, cellulose pulp was functionalized by carboxymethylation with the protocol adapted from Wagberg et al. [73]. A suspension of 30 g of cellulose pulp was prepared in water at 2 wt % and solvent exchanges were carried out in triplicate by mixing and filtration to replace water by ethanol. The amount of reagent is given by the number of equivalents of OH groups accessible onto cellulose (eq/OH). Two solutions of 1.8 eq/OH of NaOH (4.42 g) in isopropanol (136 mL) and 3 eq/OH of $ClCH_2COONa$ (17.48 g) in isopropanol (291 mL) were separately prepared by magnetic stirring. The cellulose pulp suspension in ethanol was put in the round-bottom flask, supplemented with 550 mL of isopropanol and the solution of NaOH, mechanically stirred for 30 min and heated in the oil bath at 60 °C. Then, the solution of sodium chloroacetate was added and the chemical reaction occurred for 1.5 h at 60 °C. After the carboxymethylation, the pulp was filtrated to extract isopropanol. Then, the pulp was successively washed with distilled water, a solution of acetic acid (0.1 M) and distilled water again. Finally, the modified cellulosic pulp was soaked in a solution of $NaHCO_3$ at 4 wt % for 1 h before a final washing step with distilled water. Secondly, the carboxymethylated cellulose (CMC) was mechanically fibrillated using a Masuko Grinder at 2 wt % for 1.5 h until reaching a percentage of fines superior to 99%. The amount of anionic charges was determined by conductimetric titration around 1540 ± 190 $\mu mol \cdot g^{-1}$ corresponding to a degree of oxidation around 0.26.

2.3. Elaboration of Amine-Functionalized cmNFC-Based Crosslinked Membranes

Amine-functionalized cmNFC-based crosslinked membranes were elaborated at 20 g m^{-2} with 80 wt % of cmNFC and 20 wt % of PVAm. 25.12 g of a suspension of cmNFC at 2 wt % was diluted to 0.5 wt % with distilled water and homogenized by Ultra Turrax. After adding 9.52 g of the solution of dialyzed PVAm at 1.32 wt %, the suspension was pH-adjusted at 4 with acetic acid and stirred for 20 min. A solution of 1 eq/OH of AEAPTMS (0.23 g) was previously prepared at 10 wt % in a mixture of EtOH/H_2O in 80/20 (w/w) at pH 4 and stirred for 1.5 h at room temperature before being added to the suspension. The mixture was then stirred for 5 min, filtrated on a 1-µm Nylon mesh, dried at 90 °C for 10 min and cured at 100 °C for 2 h on a sheet dryer.

2.4. Kinetics Followed by 29Si NMR Spectroscopy

All compounds and solvents were weighed directly into clean tubes. An appropriate amount of glacial acetic acid was added in D_2O to reach a pH equal to 4. AEAPTMS (10 wt %) was first added to the absolute ethanol and the zero reaction time was set immediately after the addition of acidic D_2O. The weight ratio of EtOH:D_2O was determined at 80:20. The kinetic studies were carried out directly in NMR tubes by following the evolution of the relevant NMR signals in situ. All experiments were performed by using ^{29}Si NMR spectroscopy to monitor the modification of the chemical environment of the central silicon atom of the silane molecule. The ^{29}Si NMR spectra of the silane solutions were obtained with Varian UNITY 400 and MERCURY 400 spectrometers equipped with a 10-mm BB probe operating at 79.455 MHz. This probe was used to optimize the signal-to-noise ratio, in order to minimize the acquisition times and thus follow adequately the relatively fast kinetics. All chemical shifts were measured with respect to a coaxial insert tube containing tetramethylsilane (TMS) solution as an external reference. The spectral width was 12 kHz and the relaxation delay 100 s, with proton decoupling applied only during the acquisition time in order to avoid negative NOE effects. The number of scans was increased with kinetic reaction time. The T1 measurements were made with the inversion–recovery method. The intensity of each peak (surface area) was calculated and used to construct the kinetic curves.

2.5. FTIR Spectroscopy

Infrared spectra of the membranes were determined by using a Perkin-Elmer spectrum 65. Films were analyzed with 16 scans and a resolution of 2 cm^{-1}. The baseline of the FTIR spectra was corrected and the data tuned up. Each spectrum containing NFC was normalized at 1105 cm^{-1}, which corresponds to the peak of the C-O stretching vibration of the glucopyranose ring that is not impacted by the chemical modification, and the absorbance value of this peak is set to 1 in order to qualitatively compare the intensity of the peaks from one FTIR spectrum to another.

2.6. Tensile Tests

The mechanical properties of the films were measured in an Instron Universal Testing Machine Model 4507 (Instron Engineering Corporation, Canton, MA, USA) equipped with pneumatic jaws. The properties were measured at tensile speed of 10 $mm.min^{-1}$ following the French standard NF Q 03-004 (July 1986). This testing was carried out using 10 × 1.5 cm samples from each film type after thickness measurement on average at ten locations. The samples were preconditioned at 23 °C and 50% RH.

2.7. Intrinsic Air Permeability Measurements

Air permeability was measured with a 'Mariotte system' using a permeation cell of 10 cm^2 at room temperature (25 °C and 50% RH) following the International standard ISO 5636-2:1984. The depression was imposed between 15 and 20 cm water column. Intrinsic permeability (K) was calculated following the Darcy's law Equation (1).

$$Q = \frac{K \times A \times \Delta P}{e \times \tau}, \quad (1)$$

where Q is the volume flow rate ($m^3\ s^{-1}$), K is the intrinsic permeability (m^2), A is the area tested (m^2), ΔP is the depression imposed (Pa), e is the thickness (m), and τ is the dynamic viscosity ($kg\ m^{-1}\ s^{-1}$).

2.8. Water Contact Angle Measurements

Contact angle measurements were carried out by depositing 5 µL of water droplets at the surface of the nanocellulosic substrate at room temperature. Optical Contact Angle (OCA) dataphysics system equipped with Charged Coupled Device (CCD) camera was used to record the angles between the solvent and the substrate. The acquisition of contact angle was collected for the first 60 s after deposition

2.9. Water Absorption Measurements

Water absorption measurements, commonly named Cobb60 tests, were performed using a ring of 10 cm^2 (S) and all samples were cut around the ring in order to avoid errors associated with the capillarity. The samples were first weighed (m_1), 10 mL of deionized water was added into the ring for 60 s, following the International standard ISO 535. Then, 'wet samples' were pressed once between two absorbent papers with a roll of 10 kg in order to remove residual water and weighed with a four-digit balance (m_2). The Cobb60 ($g\ m^{-2}$) was then calculated via Equation (2).

$$Cobb_{60} = \frac{m_2 - m_1}{S}, \quad (2)$$

2.10. DSC Analysis

Differential scanning calorimetry analysis was performed on cmNFC-PVAm composite materials using a DSC TA Q100-RCS instrument with Indium calibration. 5–10 mg of samples were undergone a cycle of temperature: one first heating ramp from 25 °C to 170 °C at 10 °C/min (to eliminate humidity), then a cooling ramp from 170 °C to 0 °C and finally a second heating ramp from 0 °C to 300 °C. The DSC curves were plotted from 30 °C to 300 °C during the second heating ramp with exothermic variations

in up orientation. The melting temperature (T_m) and enthalpy (H_m) were respectively determined as the temperature of the endothermic peak and by integrating the area under the endothermic curve.

2.11. Field Emission Gun-Scanning Electron Microscopy

The membranes surfaces were observed by scanning electron microscopy with a microscope ZEISS Ultra 55 equipped with a field emission gun (FEG-SEM) to get the highest picture resolution. For imaging, the samples were metallized by sputtering with about 2 nm of Au-Pd layer (Gatan PECS metallizer). Pictures were recorded at an accelerating voltage of 3 kV using in-lens detection of secondary electrons.

2.12. Energy-Dispersive X-ray Spectroscopy

Elemental analyses were performed by energy-dispersive X-ray spectroscopy (EDX) with a silicon drift detection from Bruker (SDD-30 mm^2) equipped with a detection window of light elements (5 < atomic number < 11) and using FEG-SEM microscope. Spectra of the intensity of X-radiation emitted by the sample under an electron beam were recorded in function of the energy on one point or a delimited area. Samples were metallized with 5–10 nm carbon layer to ensure their electron conductivity (Evaporateur Baltec with Carbon braiding). Spectra and X mapping were acquired with an accelerating voltage of 5 kV. The X mapping was carried out on one image and at low magnitude (x1000) for each sample to have an overview. Image processing was applied on the mapping pictures with Image J software.

2.13. Elemental Analysis

Elemental analysis was carried out by the "Institut des Sciences Analytiques (Villeurbanne, France)" of the "Centre National de la Recherche Scientifique" (CNRS). Carbon, Hydrogen, Nitrogen, Oxygen and Silicon contents were measured for neat and modified NFC. The data collected has allowed to determine the degree of substitution (DS^a) which is the number of grafted hydroxyl groups per anhydroglucose unit according to the following Equation (3) from Missoum et al. [80]

$$DS^a = \frac{6 \times M_C - \%C \times M_{AGU}}{M_{grafting} \times \%C - M_{C\ grafting}}, \quad (3)$$

where M_C is the molecular mass of Carbon (g mol^{-1}), $\%C$ is the corrected relative carbon weight content in the sample and M_{AGU}, $M_{grafting}$ and $M_{C\ grafting}$ correspond respectively to the molecular mass of anhydroglucose unit, the molecular mass of the grafted moieties and the carbon mass of the grafted moieties (all in g mol^{-1}).

2.14. Gas Permeability Measurements

Gas permeability measurements were performed with a mixed gas–continuous flow permeation cell designed in our laboratory (Figure 2). Pure gases (CO_2 or N_2) (120 Ncc/min) were fed to the system with mass flow controllers (Bronkhorst Company, Ruurlo, The Netherlands). The stream was humidified (RH = 75% and 95%) using a controlled evaporating and mixing system (Bronkhorst Control Evaporator Mixer W-202A-221-K). The total pressure of the humid feed and retentate streams were controlled by a back pressure controller (Bronkhorst Company, Ruurlo, The Netherlands) and the permeate stream was collected using a helium sweep gas with a controlled flow rate (10 Ncc/min, Bronkhorst Company, Ruurlo, The Netherlands). The permeation cell was placed in a heating cabinet (Carbolite PF030-230SN) in order to maintain a constant temperature (40 °C). All the tubing was heated with heater ropes in order to avoid any condensation in the rig.

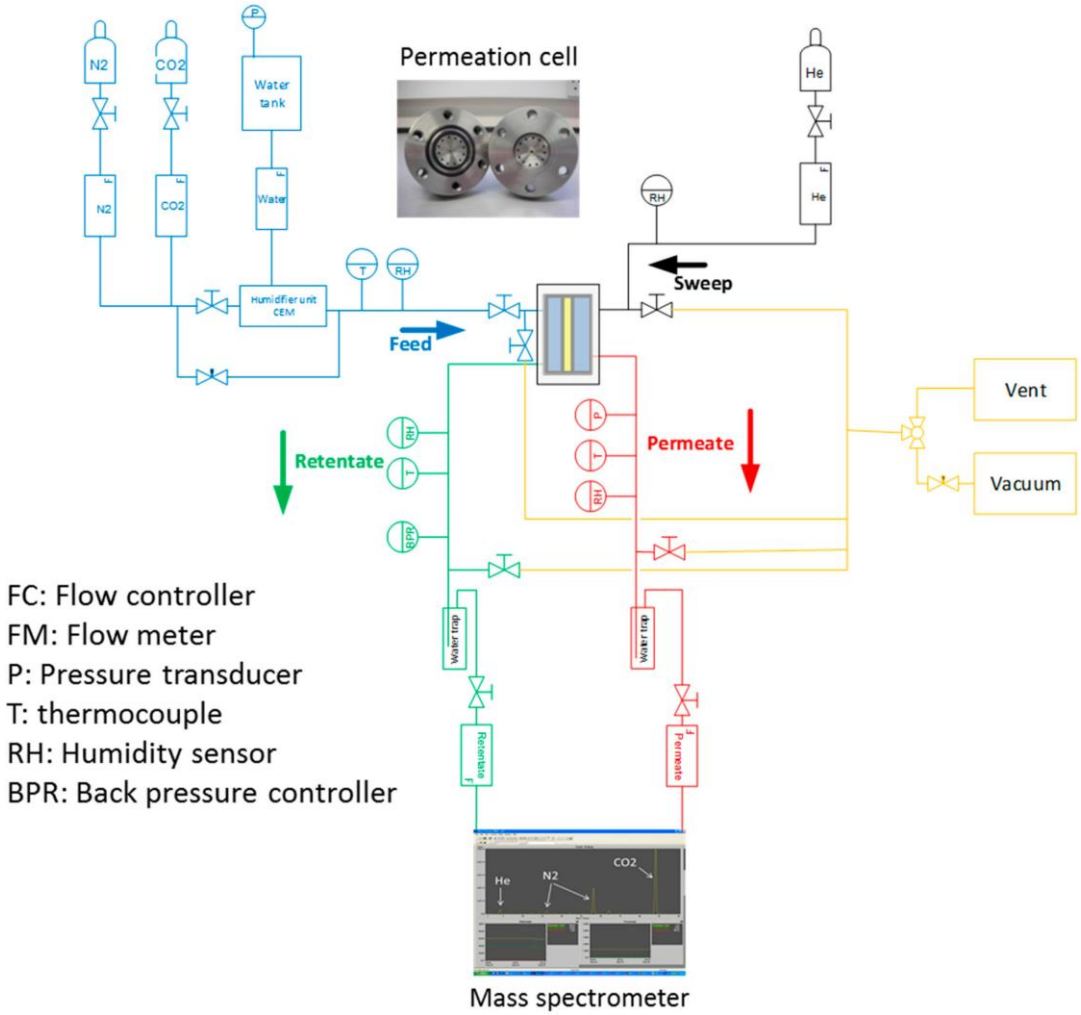

Figure 2. Mixed gas–continuous flow permeation cell.

The relative humidity and the gas concentration of the streams were measured using respectively a humidity sensor (developed in-house based on the Honeywell HIH4000 chip) and a mass spectrometer (Proline, AMETEK, Berwyn, PA, USA). The temperature of each stream was measured using a thermocouple (*K* insulated 1.5 mm thermocouple).

The temperature, the relative humidity and the gas composition of the permeate stream were recorded until the system equilibrium was reached (typically 2–3 h). The flow rates of the retentate and permeate were measured using mass flow meters (Bronkhorst Company, Ruurlo, The Netherlands), after passing through a water trap.

The permeability of each gas species passing through the membrane was calculated by

$$Perm(G) = \frac{e \cdot Flow^P \cdot X^P}{A \cdot (p^F - p^P)}, \quad (4)$$

where e is the thickness of the membrane (cm), $Flow^P$ the permeate flowrate (cm^3 (STP)/s), X^P the mole fraction of the gas in the permeate stream, A is the effective membrane area (cm^2), p^F and p^P are the partial pressure of the gas in the feed and permeate stream respectively (cmHg).

The ideal selectivity between two gas species i and j was calculated as the ratio of the two permeabilities.

$$\alpha_{ij} = \frac{Perm(i)}{Perm(j)}, \quad (5)$$

A fresh membrane was used for each experimental run that consisted in firstly the measurement of the dry mixture, and secondly the wet mixture at the chosen water vapor activity. Between two runs, the rig was evacuated until the humidity sensor detects no water, approximately 10 h.

3. Results and Discussion

3.1. Membrane Preparation

In this report, we combined cmNFC raw material and an amine-based polymer to improve the compatibility between the nanofillers and the PVAm matrix by crosslinking with the use of amine-based fixed carriers to enhance the CO_2 permeability performance. Indeed, carboxylic acid functions of the cmNFC nanofillers can react with primary amine functions of the PVAm matrix to create a new covalent bond between the filler and the matrix by amidation [77]. AEAPTMS were also grafted onto cmNFC surface to enhance the compatibility between the filler and the matrix and to add new potential site for CO_2 capture. Such membranes were elaborated according the following strategy (Figure 3). The elaboration of the membranes was performed either in a one-step process (process A) or in a two-step process (process B). In process A, all components were mixed together in one pot, whereas in process B, the crosslinking between the nanofillers and the matrix was first carried out and then the grafting of the aminosilane was performed by dipping the crosslinked membranes inside the aminosilane solution. Process A could provide different type of crosslinking reactions. Indeed, the aminosilanes can react either with their amine end-chain groups (towards -COOH groups) or their siloxanes (towards -OH groups) inducing a second network but reducing the amount of potential free $-NH_2$ site for CO_2 capture. Process B was more controlled; all the carboxylic acid functions of the cmNFC nanofiller should first react with the pendant amine functions of the PVAm matrix and then the aminosilanes should only be grafting onto -OH groups by dipping for 5 min and curing for 2 h at 100 °C [81]. The approach of crosslinking chosen consisted in first creating ionic bonds between deprotonated -COO- groups of the cmNFC and the protonated NH_3^+ at pH 4 and then forming the covalent bond by a heat-induced step at 100 °C for 2 h [81].

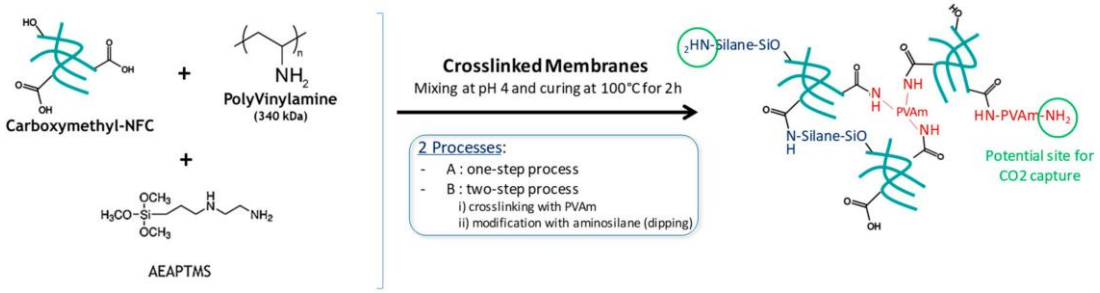

Figure 3. Strategies of elaboration of amine-functionalized cmNFC-PVAm crosslinked membranes.

The chemical modification of cmNFC with AEAPTMS was optimized by following the hydrolysis-condensation kinetics of the aminosilane in acidic D_2O/EtOH (20/80) medium followed by ^{29}Si NMR (Figure 4) [78,82,83]. Different species were observed in the reaction medium: silanes (T0R), silanols (T0H), dimers (only T1), linear oligomeric chains (T1 and T2), and 3D-chains (T1, T2, and T3). In order to simplify the evaluation of the reactivity of the aminosilane solution over time, the active silanol reactivity (Active-SiO) of the solution was proposed as a measurement parameter. This simple parameter reflected the probability of number of SiO-sites that could be grafted onto the cmNFC surface. This parameter was adapted from an empirical expression proposed by Beari et al. [84]

$$Active - SiO = \frac{(3 \times \%T0) + (2 \times \%T1) + (1 \times \%T2)}{3}, \quad (6)$$

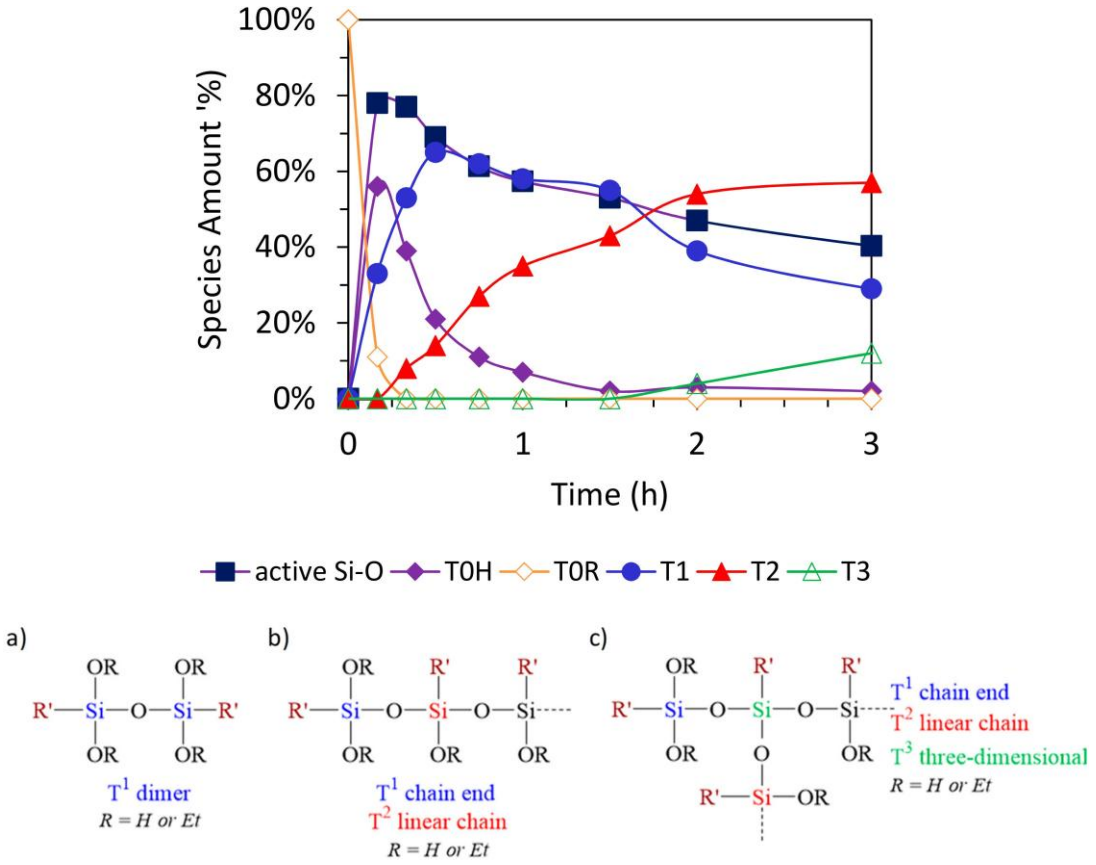

Figure 4. Hydrolysis-condensation kinetics curves of AEAPTMS in acidic D_2O/EtOH (20/80) medium followed by liquid ^{29}Si NMR in-situ. Chemical structures and assignments of the different species obtained: dimers (**a**), linear oligomers (**b**), and three-dimensional species (**c**).

We opted for the chemical hydrolysis-condensation reactions occurring for 1.5 h in order to obtain mostly linear oligomers (presence of T1 and T2 species) with a probability of grafting superior to 50% and avoiding the presence of three-dimensional T3 species.

3.2. Characterizations of the Membranes

Four membranes were studied and compared: cmNFC, cmNFC-PVAm, cmNFC-PVAm-AEAPTMS-A, and cmNFC-PVAm-AEAPTMS-B. The respective weight per surface unit and thickness of the membranes are displayed in the Table 1. The weight per surface unit was similar, around 20.9 ± 0.5 g m^{-2}, and very close to the planned value (20 g m^{-2}). The thickness varied from 23 to 35 µm. The incorporation of PVAm increased the thickness of the membranes because the water-soluble polymer might widen the distance between the nanofibers creating higher porosity.

Table 1. Characteristics of the amine-functionalized cmNFC-based crosslinked membranes.

Membranes	Weight Per Surface Unit (g m^{-2})	Thickness (µm)
cmNFC	20.3	23.3 ± 2.8
cmNFC-PVAm	21.2	35.5 ± 3.2
cmNFC-PVAm-AEAPTMS-A	21.3	34.7 ± 3.5
cmNFC-PVAm-AEAPTMS-B	20.7	30.8 ± 3.0

The FTIR spectra of amine functionalized cmNFC-PVAm membranes are showed in the Figure 5. The peaks at 1745 and 1615 cm^{-1} were respectively assigned to the stretching vibration of the C=O

carboxylic bond and the ionized C=O carboxylic bond of the cmNFC material. The broad peak at 1600–1500 cm^{-1} was assigned to the deformation vibrations of the N-H bonding of the grafted aminosilane and the PVAm [81]. Regarding the cmNFC-PVAm-AEAPTMS-B membrane elaborated from the two-step process, the broad peak assigned to N-H bonding was slightly shifted from 1580 cm^{-1} to 1530 cm^{-1} corresponding to secondary amide bonding resulting in the presence of more crosslinking of cmNFC with PVAm and/or AEAPTMS. Moreover, the peak at 1745 cm^{-1} assigned to the C=O carboxylic bond disappeared, meaning that the carboxylic acid functions have reacted assuming the crosslinking between the nanofillers and the matrix by amidation.

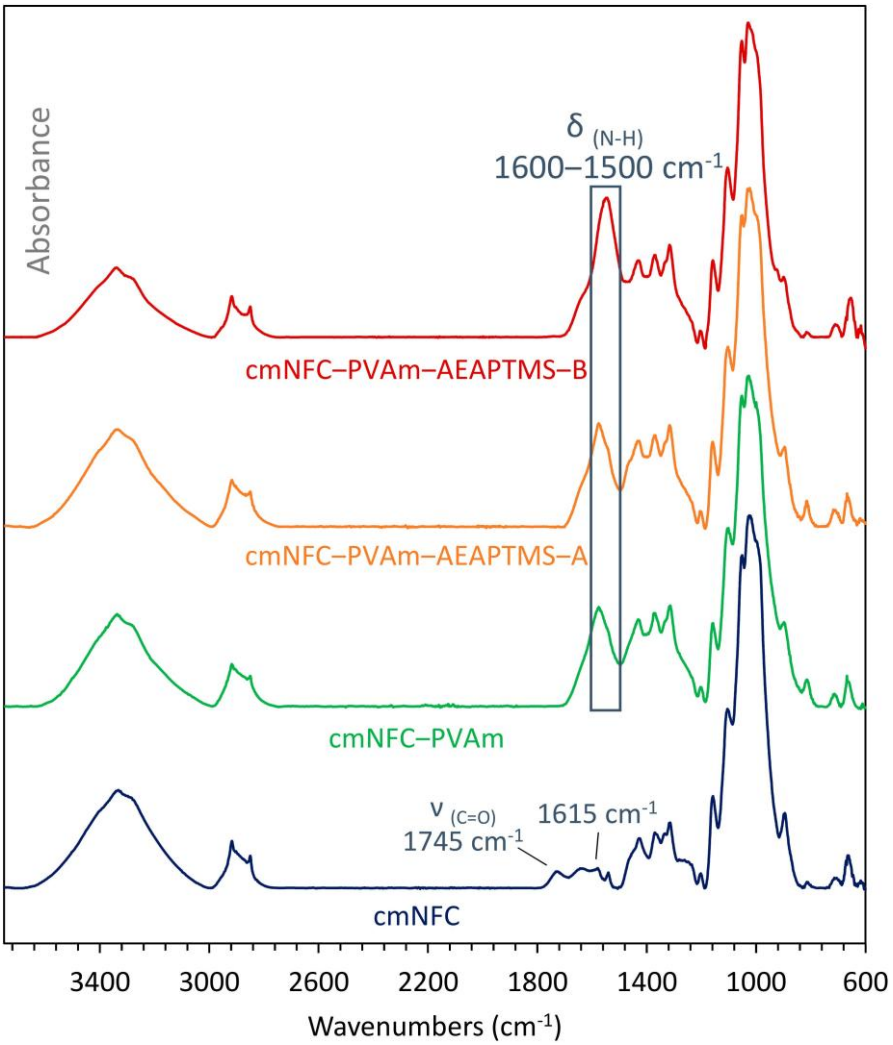

Figure 5. FTIR spectra of cmNFC, cmNFC-PVAm, and cmNFC-PVAm-AEAPTMS-A and -B membranes.

The DSC curves of the amine functionalized cmNFC-PVAm membranes are showed on Figure 6 with the corresponding melting temperatures and enthalpies in Table 2. The cmNFC nanofiller had no melting temperature and the PVAm matrix melted at around 179 °C, whereas the blends of functionalized amine or neat cmNFC and PVAm had upper melting point shifted by 46 °C. The increase in melting temperature of the PVAm inside the composite membranes was induced by a higher crystallinity of PVAm [47,85], which is a key parameter for gas transport properties. This could also prove the crosslinking between the cellulosic fillers and the polymer matrix [28] but no apparent glass–rubber transition temperature was found for the different membranes to confirm the crosslinking even at lower heating speed rate or using modulated DSC technique. Regarding the cmNFC-PVAm-AEAPTMS-B membrane elaborated from the two-step process, the melting point

was only shifted by 28 °C instead of 46 °C for the membrane elaborated with the one-step process. It also displayed a lower melting enthalpy. This difference of thermal characteristics between the two processes of membrane elaboration could be explained by: (i) the crosslinked density between the filler and the matrix was lower, (ii) there was a leakage of some free PVAm polymer chains during the step of dipping into the aqueous solution of aminosilanes (as PVAm is soluble in water), or (iii) an amorphization of the cmNFC-PVAm membranes was created by dipping the membrane inside the water-based aminosilane solution [47,85].

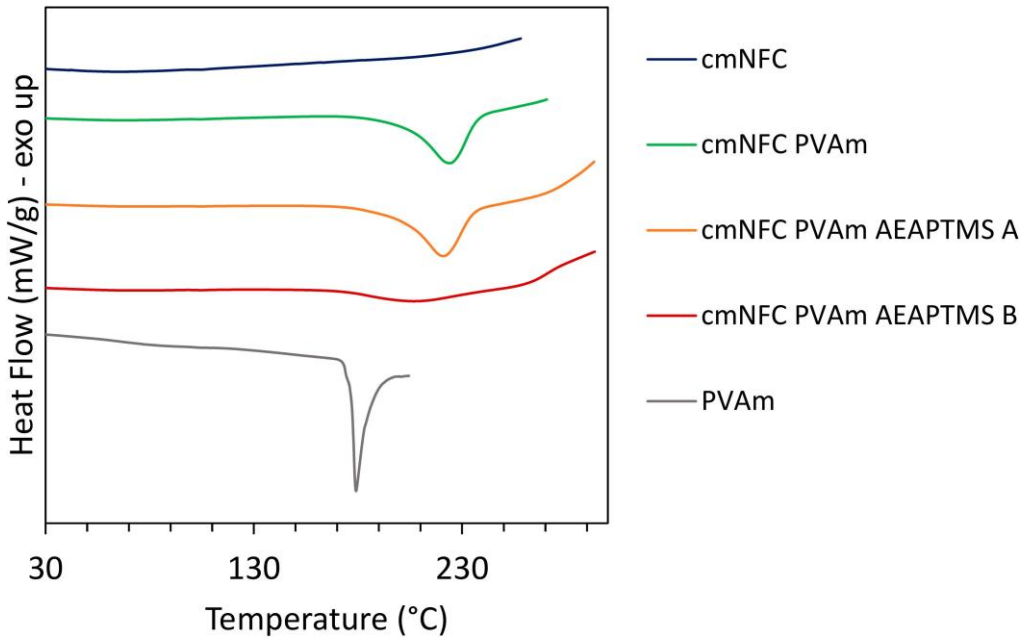

Figure 6. DSC curves of cmNFC, cmNFC-PVAm, and cmNFC-PVAm-AEAPTMS-A and -B membranes.

Table 2. Values of melting temperature (Tm) and enthalpy (Hm) obtained by DSC.

Materials	T_m (°C)	H_m (J/g)
cmNFC	-	-
PVAm	179	71.4
cmNFC-PVAm	225	96.1
cmNFC-PVAm-AEAPTMS-A	221	106.1
cmNFC-PVAm-AEAPTMS-B	207	42.3

3.3. Properties of the Membranes

Mechanical properties were determined for the neat and amine functionalized cmNFC-PVAm membranes (Figure 7a). cmNFC membranes displayed a Young's Modulus around 7.5 GPa. This modulus decreased until 6.2 GPa with the addition of PVAm which could be inconsistent with crosslinking but could be explained by the lower value of the Young's Modulus of PVAm which has less rigid polymer chain [47]. Besides, the Young's Modulus were divided by 2 when the membrane was elaborated by the two-step process. This could be explained by the dipping of the cmNFC-PVAm membranes into an aqueous solution of AEAPTMS during the second step of the elaboration of the membrane, which lowered the mechanical performance.

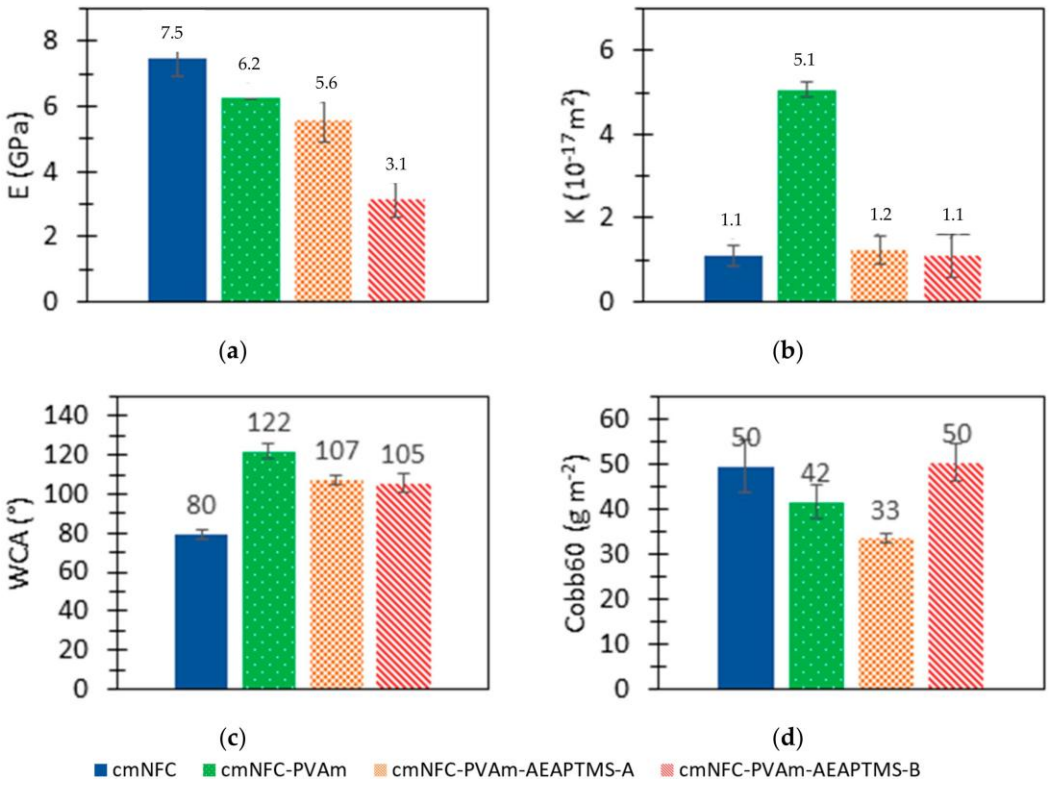

Figure 7. Properties of cmNFC, cmNFC-PVAm, cmNFC-PVAm-AEAPTMS-A and -B membranes: Young's modulus (**a**), intrinsic air permeability (**b**), water contact angle (**c**), and Cobb60 measurements (**d**).

The intrinsic air permeability was measured for the neat and amine functionalized cmNFC-PVAm membranes (Figure 7b). cmNFC membranes displayed an intrinsic air permeability value around 1.1 10^{-17} m^2. The intrinsic air permeability was multiplied by around 5 with the addition of PVAm. This observation confirmed that PVAm has a higher permeance that pure cmNFC films. The polymer chains were dispersed in the cmNFC network and increased the distance between the nanofibers. The network was less dense and the pore size slightly increased. Consequently, air can cross the membrane more easily. On the contrary, the addition of aminosilane improved the barrier properties of the membranes against air with similar results to cmNFC membrane is probably because of the formation of a denser second network.

The water contact angle (WCA) on the upper surface of the neat and amine functionalized cmNFC-PVAm membranes was measured (Figure 7c). The WCA value on cmNFC surface was measured at 80° confirming that the surface was still hydrophilic due to the presence of carboxylic acid functions on the surface of the nanofibers. The WCA values of the films prepared with amine-functionalized cmNFC-PVAm were above 90°—around 105° for both membranes—meaning that the surface of the films became hydrophobic despite their hydrophilic amines groups, which reinforced the hypothesis that the amine groups have reacted. The addition of PVAm enhanced the hydrophobicity of the surface with WCA values around 120° due to the presence of grafted linear polymer chains with an olefin backbone.

The liquid water absorption measurements (Cobb60) on neat and amine-functionalized cmNFC-PVAm membranes are showed on Figure 7d. The Cobb60 value for cmNFC membrane was high around 50 g m^{-2}. Despite their hydrophobic surface, the membranes absorbed a large amount of liquid water with Cobb60 value above 30 g m^{-2}, since PVAm has a good affinity to water. Moreover, a visual swelling of the membranes in presence of liquid water was observed while the

integrity of the sample remained intact. This observation supports the crosslinking effect between the filler and the matrix as suggested.

3.4. Morphology of the Membranes and Elemental Quantification

The SEM pictures of neat and amine-functionalized cmNFC based membranes are showed on Figure 8 and observed on the top surface. The diameter of the individual cmNFC fibers was estimated between 10 and 30 nm. Nanopores were observed on the cmNFC films. The diameter of the nanopores was estimated at 24 ± 10 nm (calculation by Image J from FEG-SEM pictures (x30,000) over 100 pores). No nanoporosity was observed for cmNFC-PVAm and cmNFC-PVAm-AEAPTMS-A in one-step process maybe due to the covering of the nanopores by the polymer. However, nanoporosity was observed for the membrane cmNFC-PVAm-AEAPTMS-B elaborated in a two-step process. The diameter of the nanopores was estimated at 22 ± 9 nm (similar to cmNFC nanopores diameter). The step of dipping inside water in two-step process might cause the solubilization of free PVAm polymer chains and generated nanoporosity as observed for cmNFC.

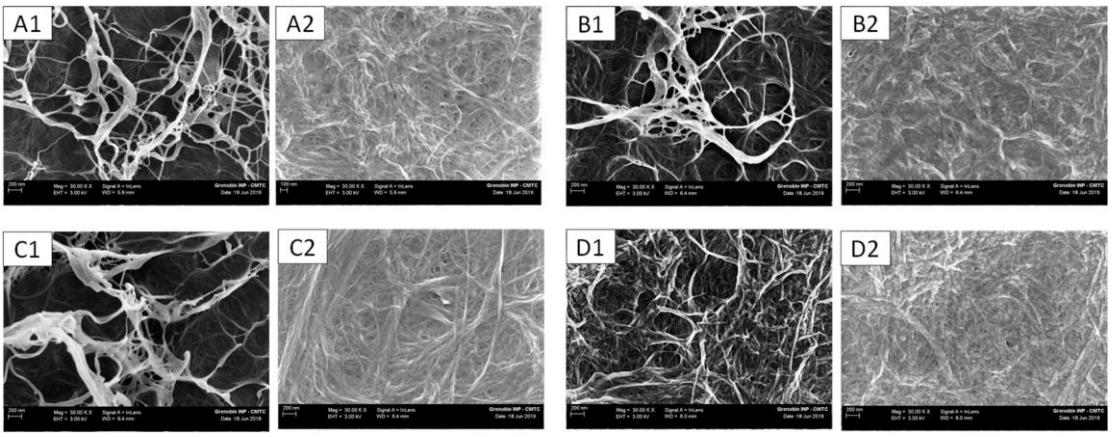

Figure 8. FEG-SEM pictures of cmNFC (**Ai**), cmNFC-PVAm (**Bi**), cmNFC-PVAm-AEAPTMS-A (**Ci**), and cmNFC-PVAm-AEAPTMS-B (**Di**) on individual fibers (**i = 1**) and surface (**i = 2**) [x30,000].

The FEG-SEM pictures with EDX mapping on C, O, N, and Si elements of cmNFC, cmNFC-PVAm, and cmNFC-PVAm-AEAPTMS-A and -B with the corresponding EDX spectra are showed on Figure 9. The elemental semi-quantitative calculation from FEG-SEM-EDX characterization was reported on Table 3. All the membranes presented the characteristic C and O elements of cellulose respectively observed at 0.28 and 0.53 keV. The $I_{O/C}$ value of the cmNFC film was lower than the theoretical one (expected at 0.83) certainly because of the carbon layer deposited on the film essential for the EDX characterization. The membranes containing PVAm polymer displayed the characteristic peak of N element at 0.39 keV with good dispersion of the element on the mapping pictures. This result proved the effective dispersion of the polymer matrix inside the membranes. The N atomic percentages were similar (around 11 ± 1%) since the same amount of PVAm was used and the $I_{O/C}$ value decreased because only C and N elements were added by the polymer in the calculation. The presence of the aminosilane was observed with the appearance of the Si peak at 1.74 keV and some Si dots spread out on the mapping pictures for both one-step and two-step processes. However, its intensity was low and its atomic percentage close to the detection limit of the apparatus, but the one-step process seemed to be better for the grafting of the aminosilane with higher Si content. Traces of Na and Cl elements were also observed on the EDX spectra, which were originated from tap water used to prepare cmNFC.

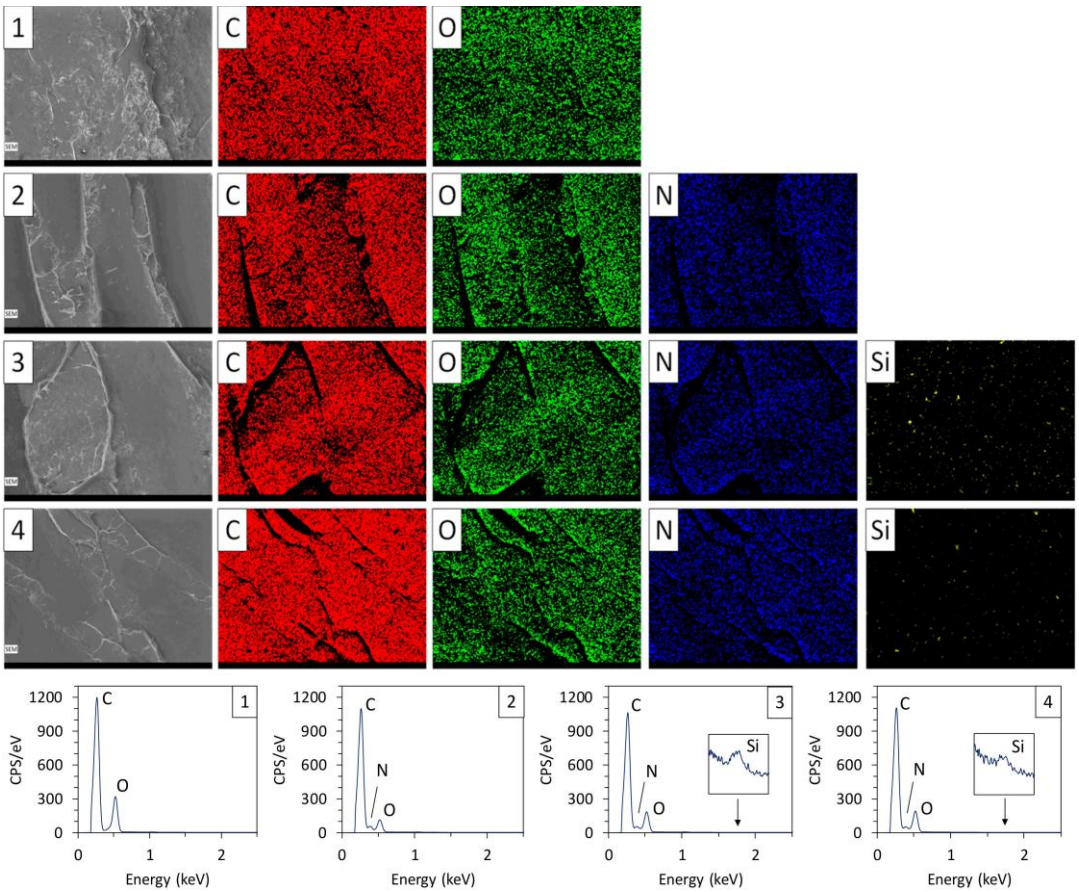

Figure 9. FEG-SEM pictures with EDX mapping on Carbon, Oxygen, Nitrogen and Silicon elements of cmNFC (**1**), cmNFC-PVAm (**2**), and cmNFC-PVAm-AEAPTMS-A (**3**) and -B (**4**) surfaces. Spectra of the intensity of X-radiation emitted by the sample under an electron beam were also presented in function of the energy on the delimited area of the membranes with the assignment of the energy of the different elements.

Table 3. Elemental semi-quantitative calculation from FEG-SEM-EDX characterization with atomic percentage of each element and their intensity with respect to carbon.

Materials	% C	% O	% N	% Si	$I_{O/C}$	$I_{N/C}$	$I_{Si/C}$
cmNFC	62.1	37.9	-	-	0.56	-	-
cmNFC-PVAm	63.6	24.3	12.2	-	0.32	0.09	-
cmNFC-PVAm-AEAPTMS-A	62.0	26.7	11.1	0.2	0.36	0.08	0.005
cmNFC-PVAm-AEAPTMS-B	62.6	26.8	10.4	0.1	0.36	0.08	0.003

The elemental analyses of C, H, O, N, and Si atoms were performed on cmNFC, cmNFC-PVAm, and cmNFC-PVAm-AEAPTMS-A and -B membranes. The results in terms of elemental weight concentration are summarized in Table 4. The proportion in oxygen in all samples was higher than the theoretical value. The difference could be explained by the presence of some O-rich impurities and by experimental errors [86]. The degree of substitution of OH groups from cellulose by COOH in cmNFC materials was estimated at 0.32 using the Equation (3) and was very close to the value of the degree of oxidation equal to 0.26 obtained by titration for cmNFC with 1540 µmol g^{-1} as charges rate. The degree of substitution of the COOH groups from cmNFC by amide functions obtained by the crosslinking between cmNFC and PVAm was calculated using the following equation adapted from Equation (3)

$$DS^b = \frac{12 \times M_C - \%C \times M_{AGU}{}^{cmNFC}}{M_{grafting} \times \%C - M_{C\ grafting}}, \quad (7)$$

where 12 is the number of carbon in the anhydroglucose unit of fully substituted cmNFC, M_C is the molecular mass of Carbon ($g \cdot mol^{-1}$), $\%C$ is the corrected relative carbon weight content in the sample and M_{AGU}^{cmNFC}, $M_{grafting}$, and $M_{C\ grafting}$ correspond respectively to the molecular mass of anhydroglucose unit for totally substituted cmNFC, the molecular mass of a PVAm unit and the Carbon mass of a PVAm unit.

Table 4. Elemental weight concentration of each element obtained by elemental analysis.

Samples	Elemental Weight Concentration					DS [a,b]
	%C	%O	%H	%N	%Si	
cmNFC	44.1 (*44.1*) *	50.0 (*49.8*) *	5.9 (*6.0*) *	0.0 (-) *	- (-) *	0.32 [a]
cmNFC-PVAm	44.0 (*46.6*) *	41.5 (*39.7*) *	8.1 (*7.1*) *	6.4 (*6.5*) *	- (-) *	0.76 [b]
cmNFC-PVAm-AEAPTMS-A	43.8 (*43.4*) *	42.4 (*36.6*) *	7.6 (*7.6*) *	6.1 (*8.7*) *	0.1 (*3.8*) *	0.64 [b]
cmNFC-PVAm-AEAPTMS-B	44.2 (*43.4*) *	42.8 (*36.6*) *	7.8 (*7.6*) *	5.0 (*8.7*) *	0.2 (*3.8*) *	0.92 [b]

* (theoretical values), DS [a,b] values relative to carboxymethyl groups [a] or amide groups [b].

The degree of substitution for cmNFC-PVAm-based membranes was estimated at 0.76, 0.64, and 0.92 respectively for cmNFC-PVAm, cmNFC-PVAm-AEAPTMS-A, and cmNFC-PVAm-AEAPTMS -B. The maximum of degree of substitution is equal to 3 for 100% of substituted moieties. Indeed, there are three OH groups per anhydroglucose unit of the cellulose that could be substituted. So, the results led to 25 ± 5% of COOH moieties from cmNFC have been crosslinked with PVAm whatever the process. Unfortunately, the detected amount of Si was very low compared to the theoretical value. The process A and B did not allow to correctly graft the aminosilanes onto the cellulosic substrate probably because of less competitive reaction kinetics compared to the PVAm crosslinking, steric hindrance, less reactive available functions, and/or the filtration step.

3.5. Separation Performance

The permeability coefficients of pure CO_2 and N_2 have been determined for two different feed humidity contents (75% and 95%) at 40 °C and 1.5 bar. The Table 5 summarized the permeation data for the pure and modified cmNFC-based membranes mixed with 20% PVAm.

Table 5. Permeation data for cmNFC, cmNFC-PVAm, cmNFC-PVAm, AEAPTMS-A and cmNFC-PVAm-AEAPTMS-B at 40 °C and 1.5 bar (Error calculated by sample repetition).

	PermCO₂[Barrer] [+/−5%]		Selectivity CO_2/N_2	
	RH = 75%	RH = 95%	RH = 75%	RH = 95%
cmNFC [64]	3	40	25	56
cmNFC-PVAm	10	50	20	71
cmNFC-PVAm-AEAPTMS-A	20	92	40	131
cmNFC-PVAm-AEAPTMS-B	20	90	40	128

The gas transport properties of cmNFC were relevantly affected by the water content within the membrane matrix. The Table 5 showed that at RH = 75% the membrane presented low CO_2 permeability, 3 Barrer, whereas at high humidity content the permeability increased by 15 times, reaching a value of 40 Barrer. For hydrophilic materials, such as cmNFC, the presence of water

induced an increase in gas permeability due to an extensive swelling and dilation of the membrane. The ideal selectivity for CO_2/N_2 pairs increased also along with the water content in the membrane. The N_2 permeability seemed to be less affected by the water content due larger kinetic size and smaller solubility in water [52].

The addition of PVAm had a positive effect on the separation performance. The presence of PVAm induced an increase in CO_2 permeability, with a noticeable improvement at the lower humidity content. At 75% of humidity, the CO_2 permeability coefficient was increased by 233%, whereas at 95%, it was only by 25%. The addition of PVAm brought hydrophobicity, which induced clusters formation of water and a decrease of gas transport at high water content. The same behavior has been observed by Ansaloni et al. [52], the permeability of their MFC-Lupamine nanocomposite appeared to be less affected by the water content in the high activity range. The selectivity for CO_2/N_2 pairs increased as well with the presence of PVAm within cmNFC but only by 27%, which could be related to higher air permeability of the cmNFC-PVAm membrane.

When cmNFC was crosslinked with PVAm and aminosilanes, a clear enhancement of the separation performance was observed with respect to pure cmNFC membranes. The CO_2 permeability coefficient reached a maximum value of 92 Barrer and 90 Barrer at 95% RH, for cmNFC-PVAm-AEAPTMS-A and cmNFC-PVAm-AEAPTMS-B respectively. This improvement was due to the presence of the amino group which could react with CO_2 molecules. As the EDX and elemental analysis showed, the percentage of grafted amino group were similar for the two processes, which was consistent with the fact that the sample A and B had a similar CO_2 permeability coefficient. Similarly to the cmNFC-PVAm membrane, the presence of water in the membrane induced a large increase in the CO_2 permeability, but with a lower impact as pure cmNFC, due to the hydrophobicity of PVAm and aminosilanes. The selectivity for CO_2/N_2 was also improved by the crosslinking with values 2.3 times larger than what observed in pure MFC. In particular, at the high humidity content, the selectivity grew from 56 to 130. Actually, the presence of water enhanced the ideal selectivity. As said before, the N_2 permeability was less affected by the water content within the membrane.

4. Conclusions

The compatibility between an amine-based polymer and a cellulosic carboxymethylated nanofillers was enhanced by a crosslinking reaction. The process of the functionalization of cmNFC with AEAPTMS was optimized by following their hydrolysis-condensation kinetics in ^{29}Si NMR spectroscopy. The membranes were less sensitive to liquid water and the crystallinity of PVAm was tuned by the conditions of the membrane elaboration. Around 25% of the -COOH functions from cmNFC have crosslinked with PVAm. Unfortunately, the introduction of PVAm during the process disrupted the grafting reaction of AEAPTMS as they reacted with the same function. Only a few grafted aminosilane oligomers were detected. Nevertheless, the presence of PVAm and aminosilane allowed to obtain better CO_2 permeability and CO_2/N_2 selectivity at a given high water concentration in the membrane suggesting the existence of a facilitation effect due to amine-CO_2 interaction, while the mechanical integrity of the membranes remained intact. These stable bio sourced membranes were proposed as good candidates to be tested in real conditions in the framework of the European NanoMEMC^2 collaborative project.

Author Contributions: Conceptualization, B.D.; Data curation, B.D. and E.L.; Formal analysis, B.D., E.L., and M.-C.B.-S.; Investigation, B.D., E.L., and K.M.; Methodology, B.D. and K.M.; Project administration, B.D.; Resources, B.D. and E.L.; Supervision, M.-C.F. and K.M.; Validation, B.D., E.L., M.-C.B.-S., M.-C.F., and K.M.; Writing—original draft preparation, B.D.; Writing—review and editing, B.D., E.L., M.-C.B.-S., and M.-C.F. All authors have read and agreed to the published version of the manuscript.

Funding: This research was funded by the European Commission within the NanoMEMC^2 project. This project received funding from the European Union's Horizon 2020 Research and Innovation program under grant agreement no. 727734.

Acknowledgments: The authors are grateful to Francine ROUSSEL-DHERBEY from the structural microscopy platform in C.M.T.C. (Consortium des Moyens Technologiques Communs—Insitut Polytechnique de Grenoble) for the FEG-SEM and EDX analyses.

Conflicts of Interest: The authors declare no conflict of interest. The funders had no role in the design of the study; in the collection, analyses, or interpretation of data; in the writing of the manuscript, or in the decision to publish the results.

References

1. Earth System Research Laboratory Global Monitoring Division. Available online: https://www.esrl.noaa.gov/gmd/ccgg/trends/full.html (accessed on 8 May 2019).
2. Aaron, D.; Tsouris, C. Separation of CO_2 from Flue Gas: A Review. *Sep. Sci. Technol.* **2005**, *40*, 321–348. [CrossRef]
3. D'Alessandro, D.M.; Smit, B. Carbon Dioxide Capture. *Angew. Chem. Int. Ed.* **2010**, *49*, 6058–6082. [CrossRef] [PubMed]
4. Baker, R.W. Future Directions of Membrane Gas Separation Technology. *Ind. Eng. Chem. Res.* **2002**, *41*, 1393–1411. [CrossRef]
5. Lee, A.L.; Feldkirchner, H.L.; Stern, S.A.; Houde, A.Y.; Gamez, J.P.; Meyer, H.S. Field tests of membrane modules for the separation of carbon dioxide from low-quality natural gas. *Gas Sep Purif.* **1995**, *9*, 35. [CrossRef]
6. Bernardo, P.; Clarizia, G. 30 Years of Membrane Technology for Gas Separation. *Chem. Eng.* **2013**, *32*, 1999–2004.
7. Favre, E. Carbon dioxide recovery from post-combustion processes: Can gas permeation membranes compete with absorption? *J. Membr. Sci.* **2007**, *294*, 50–59. [CrossRef]
8. Bernardo, P.; Drioli, E.; Golemme, G. Membrane gas separation: 1 review of state of the art. *Ind. Chem. Eng.* **2009**, *48*, 4638–4663. [CrossRef]
9. Khalilpour, R.; Mumford, K.; Zhai, H.; Abbas, A.; Stevens, G.; Rubin, E.S. Membrane-based carbon capture from flue gas: A review. *J. Clean. Prod.* **2015**, *103*, 286–300. [CrossRef]
10. Baker, R.W.; Lokhandwala, K. Natural Gas Processing with Membranes: An Overview. *Ind. Eng. Chem. Res.* **2008**, *47*, 2109–2121. [CrossRef]
11. Robeson, L.M. The upper bound revisited. *J. Membr. Sci.* **2008**, *320*, 390–400. [CrossRef]
12. Wijmans, J.G.; Baker, R.W. The Solution-Diffusion Model—A Review. *J. Membr. Sci.* **1995**, *107*, 1–21. [CrossRef]
13. Fernández-Barquín, A.; Rea, R.; Venturi, D.; Giacinti-Baschetti, M.; De Angelis, M.G.; Casado-Coterillo, C.; Irabien, Á. Effect of relative humidity on the gas transport properties of zeolite A/PTMSP mixed matrix membranes. *RSC Adv.* **2018**, *8*, 3536–3546. [CrossRef]
14. Rezakazemi, M.; Ebadi Amooghin, A.; Montazer-Rahmati, M.M.; Ismail, A.F.; Matsuura, T. State-of-the-art membrane based CO_2 separation using mixed matrix membranes (MMMs): An overview on current status and future directions. *Prog. Polym. Sci.* **2014**, *39*, 817–861. [CrossRef]
15. Mahmoudi, A.; Asghari, M.; Zargar, V. CO2/CH4 separation through a novel commercializable three-phase PEBA/PEG/NaX nanocomposite membrane. *J. Ind. Eng. Chem.* **2015**, *23*, 238–242. [CrossRef]
16. Chen, Y.; Wang, B.; Zhao, L.; Dutta, P.; Winston Ho, W.S. New Pebax®/zeolite Y composite membranes for CO_2 capture from flue gas. *J. Membr. Sci.* **2015**, *495*, 415–423. [CrossRef]
17. Nafisi, V.; Hägg, M.B. Development of dual layer of ZIF-8/PEBAX-2533 mixed matrix membrane for CO_2 capture. *J. Membr. Sci.* **2014**, *459*, 244–255. [CrossRef]
18. Scholes, C.A.; Bacus, J.; Chen, G.Q.; Tao, W.X.; Li, G.; Qader, A.; Stevens, G.W.; Kentish, S.E. Pilot plant performance of rubbery polymeric membranes for carbon dioxide separation from syngas. *J. Membr. Sci.* **2012**, *389*, 470–477. [CrossRef]
19. Tena, A.; Shishatskiy, S.; Filiz, V. Poly(ether-amide) vs. poly(ether-imide) copolymers for post-combustion membrane separation processes. *RSC Adv.* **2015**, *5*, 22310–22318. [CrossRef]
20. Matsuyama, H.; Teramoto, M.; Sakakura, H.; Iwai, K. Facilitated transport of CO_2 through various ion exchange membranes prepared by plasma graft polymerization. *J. Membr. Sci.* **1996**, *117*, 251–260. [CrossRef]
21. Matsuyama, H.; Terada, A.; Nakagawara, T.; Kitamura, Y.; Teramoto, M. Facilitated transport of CO_2 through polyethylenimine/poly(vinyl alcohol) blend membrane. *J. Membr. Sci.* **1999**, *163*, 221–227. [CrossRef]

22. Noble, R.D. Generalized microscopic mechanism of facilitated transport in fixed site carrier membranes. *J. Membr. Sci.* **1992**, *75*, 121–129. [CrossRef]
23. Ward, W.J.; Robb, W.L. Carbon dioxide-oxygen separation: Facilitated transport of carbon dioxide across a liquid film. *Science* **1967**, *156*, 1481–1484. [CrossRef] [PubMed]
24. Huang, J.; Zou, J.; Ho, W.S.W. Carbon Dioxide Capture Using a CO_2—Selective Facilitated Transport Membrane. *Ind. Eng. Chem. Res.* **2008**, *47*, 1261–1267. [CrossRef]
25. Rea, R.; De Angelis, M.G.; Baschetti, M.G. Models for facilitated transport membranes: A review. *Membranes* **2019**, *9*, 26. [CrossRef]
26. Teramoto, M.; Huang, Q.; Maki, T.; Matsuyama, H. Facilitated transport of SO_2 through supported liquid membrane using water as a carrier. *Sep. Purif. Technol.* **1999**, *16*, 109–118. [CrossRef]
27. Matsuyama, H.; Teramoto, M.; Sakakura, H. Selective permeation of CO_2 through poly 2-(N,Ndimethyl) aminoethyl methacrylate membrane prepared by plasma-graft polymerization technique. *J. Membr. Sci.* **1996**, *114*, 193–200. [CrossRef]
28. Deng, L.; Kim, T.J.; Hägg, M.B. Facilitated transport of CO_2 in novel PVAm/PVA blend membrane. *J. Membr. Sci.* **2009**, *340*, 154–163. [CrossRef]
29. Kim, T.J.; Baoan, L.I.; Hägg, M.B. Novel fixed-site-carrier polyvinylamine membrane for carbon dioxide capture. *J. Polym. Sci. Part B Polym. Phys.* **2004**, *42*, 4326–4336. [CrossRef]
30. Zhao, Y.; Winston Ho, W.S. Steric hindrance effect on amine demonstrated in solid polymer membranes for CO2 transport. *J. Membr. Sci.* **2012**, *415*, 132–138. [CrossRef]
31. Tong, Z.; Ho, W.S.W. New sterically hindered polyvinylamine membranes for CO_2 separation and capture. *J. Membr. Sci.* **2017**, *543*, 202–211. [CrossRef]
32. Sandru, M.; Kim, T.J.; Hägg, M.B. High molecular fixed-site-carrier PVAm membrane for CO_2 capture. *Desalination* **2009**, *240*, 298–300. [CrossRef]
33. Caplow, M. Kinetics of carbamate formation and breakdown. *J. Am. Chem. Soc.* **1968**, *90*, 6795–6803. [CrossRef]
34. Ward, W.J. Facilitated Transport Liquid Membrane. US Patent 3,676,220, 11 July 1972.
35. Kovvali, A.S.; Sirkar, K.K. Dendrimer Liquid Membranes: CO_2 Separation from Gas Mixtures. *Ind. Eng. Chem. Res.* **2001**, *40*, 2502–2511. [CrossRef]
36. Li, F.; Li, Y.; Chung, T.-S.; Kawi, S. Facilitated transport by hybrid POSS®–Matrimid®–Zn^{2+} nanocomposite membranes for the separation of natural gas. *J. Membr. Sci.* **2010**, *356*, 14–21. [CrossRef]
37. Matsuyama, H.; Teramoto, M.; Iwau, K. Development of a new functional cation-exchange membrane and its application to facilitated transport of CO_2. *J. Membr. Sci.* **1994**, *93*, 237–244. [CrossRef]
38. Matsuyama, H.; Hirai, K.; Teramoto, M. Selective permeation of carbon dioxide through plasma polymerized membrane from diisopropylamine. *J. Membr. Sci.* **1994**, *92*, 257–265. [CrossRef]
39. Yoshikawa, M.; Ezaki, T.; Sanui, K.; Ogata, N. Selective permeation of carbon dioxide through synthetic polymer membranes having pyridine moiety as a fixed carrier. *J. Appl. Polym. Sci.* **1988**, *35*, 145–154. [CrossRef]
40. Yoshikawa, M.; Fujimoto, K.; Kinugawa, H.; Kitao, T.; Ogata, N. Selective Permeation of Carbon Dioxide through Synthetic Polymeric Membranes Having Amine Moiety. *Chem. Lett.* **1994**, *23*, 243–246. [CrossRef]
41. Yamaguchi, T.; Boetje, L.M.; Koval, C.A.; Noble, R.D.; Bowman, C.N. Transport Properties of Carbon Dioxide through Amine Functionalized Carrier Membranes. *Ind. Eng. Chem. Res.* **1995**, *34*, 4071. [CrossRef]
42. Yamaguchi, T.; Koval, C.A.; Noble, R.D.; Bowman, C.N. Transport mechanism of carbon dioxide through perfluorosulfonate ionomer membranes containing an amine carrier. *Chem. Eng. Sci.* **1996**, *51*, 4781. [CrossRef]
43. Ho, W.W.; Li, K. Recent advances in separations. *Curr. Opin. Chem. Eng.* **2013**, *2*, 207–208. [CrossRef]
44. Ansaloni, L.; Zhao, Y.; Jung, B.T.; Ramasubramanian, K.; Baschetti, M.G.; Ho, W.S.W. Facilitated transport membranes containing amino-functionalized multi-walled carbon nanotubes for high-pressure CO_2 separations. *J. Memb. Sci.* **2015**, *490*, 96–102. [CrossRef]
45. Zhang, Y.; Sunarso, J.; Liu, S.; Wang, R. Current status and development of membranes for CO_2/CH_4 separation: A review. *Int. J. Greenh. Gas Control* **2013**, *12*, 84–107. [CrossRef]
46. Deng, L.; Hägg, M.-B. Carbon nanotube reinforced PVAm/PVA blend FSC nanocomposite membrane for CO_2/CH_4 separation. *Int. J. Greenh. Gas Control* **2014**, *26*, 127–134. [CrossRef]

47. He, Y.; Wang, Z.; Dong, S.; Zhao, S.; Qiao, Z.; Cao, X.; Wang, J.; Wang, S. Polymeric composite membrane fabricated by 2-aminoterephthalic acid chemically crosslinked polyvinylamine for CO_2 separation under high temperature. *J. Membr. Sci.* **2016**, *518*, 60–71. [CrossRef]
48. Zou, J.; Ho, W.S.W. CO_2-selective polymeric membranes containing amines in crosslinked poly(vinyl alcohol). *J. Membr. Sci.* **2006**, *286*, 310–321. [CrossRef]
49. He, X.; Kim, T.J.; Hägg, M.B. Hybrid fixed-site-carrier membranes for CO_2 removal from high pressure natural gas: Membrane optimization and process condition investigation. *J. Membr. Sci.* **2014**, *470*, 266–274. [CrossRef]
50. Deng, L.; Kim, T.J.; Hägg, M.B. PVA/PVAm blend FSC membrane for CO_2-capture. *Desalination* **2006**, *199*, 523–524. [CrossRef]
51. Zhao, Y.; Jung, B.T.; Ansaloni, L.; Ho, W.S.W. Multiwalled carbon nanotube mixed matrix membranes containing amines for high pressure CO_2/H_2 separation. *J. Membr. Sci.* **2014**, *459*, 233–243. [CrossRef]
52. Ansaloni, L.; Salas-Gay, J.; Ligi, S.; Baschetti, M.G. Nanocellulose-based membranes for CO_2 capture. *J. Membr. Sci.* **2017**, *522*, 216–225. [CrossRef]
53. Venturi, D.; Ansaloni, L.; Baschetti, M.G. Nanocellulose based facilitated transport membranes for CO_2 separation. *Chem. Eng. Trans.* **2016**, *47*, 349–354. [CrossRef]
54. Chen, Y.; Ho, W.S.W. High-molecular-weight polyvinylamine/piperazine glycinate membranes for CO_2 capture from flue gas. *J. Membr. Sci.* **2016**, *514*, 376–384. [CrossRef]
55. Turbak, A.F.; Snyder, F.W.; Sandberg, K.R. Microfibrillated cellulose, a new cellulose product: Properties, and commercial potential. In Proceedings of the Conference: 9. Cellulose Conference, Syracuse, Syracuse, NY, USA, 24 May 1982.
56. Dufresne, A. Nanocellulose: A new ageless bionanomaterial. *Mater. Today* **2013**, *16*, 220–227. [CrossRef]
57. Nechyporchuk, O.; Belgacem, M.N.; Bras, J. Production of cellulose nanofibrils: A review of recent advances. *Ind. Crops Prod.* **2016**, *93*, 2–25. [CrossRef]
58. Lavoine, N.; Desloges, I.; Dufresne, A.; Bras, J. Microfibrillated cellulose—Its barrier properties and applications in cellulosic materials: A review. *Carbohydr. Polym.* **2012**, *90*, 735–764. [CrossRef]
59. Klemm, D.; Kramer, F.; Moritz, S.; Lindström, T.; Ankerfors, M.; Gray, D.; Dorris, A. Nanocelluloses: A new family of nature-based materials. *Angew. Chem. Int. Ed.* **2011**, *50*, 5438–5466. [CrossRef]
60. Brodin, F.W.; Gregersen, Ø.W.; Syverud, K. Cellulose nanofibrils: Challenges and possibilities as a paper additive or coating material—A review. *Nord. Pulp Pap. Res. J.* **2014**, *29*, 156–166. [CrossRef]
61. Oksman, K.; Aitomäki, Y.; Mathew, A.P.; Siqueira, G.; Zhou, Q.; Butylina, S.; Tanpichai, S.; Zhou, X.; Hooshmand, S. Review of the recent developments in cellulose nanocomposite processing. *Compos. Part A Appl. Sci. Manuf.* **2016**, *83*, 2–18. [CrossRef]
62. Hoeng, F.; Denneulin, A.; Bras, J. Use of nanocellulose in printed electronics: A review. *Nanoscale* **2016**, *8*, 13131–13154. [CrossRef]
63. Jorfi, M.; Foster, E.J. Recent advances in nanocellulose for biomedical applications. *J. Appl. Polym. Sci.* **2015**, *132*, 1–19. [CrossRef]
64. Venturi, D.; Chrysanthou, A.; Dhuiège, B.; Missoum, K.; Baschetti, M.G. Arginine/Nanocellulose Membranes for Carbon Capture Applications. *Nanomaterials* **2019**, *9*, 877. [CrossRef] [PubMed]
65. Venturi, D.; Grupkovic, D.; Sisti, L.; Baschetti, M.G. Effect of humidity and nanocellulose content on Polyvinylamine-nanocellulose hybrid membranes for CO_2 capture. *J. Membr. Sci.* **2018**, *548*, 263–274. [CrossRef]
66. Torstensen, J.; Helberg, R.M.L.; Deng, L.; Gregersen, Ø.W.; Syverud, K. PVA/nanocellulose nanocomposite membranes for CO_2 separation from flue gas. *Int. J. Greenh. Gas Control* **2019**, *81*, 93–102. [CrossRef]
67. Pääkko, M.; Ankerfors, M.; Kosonen, H.; Nykänen, A.; Ahola, S.; Österberg, M.; Ruokolainen, J.; Laine, J.; Larsson, P.T.; Ikkala, O. Enzymatic hydrolysis combined with mechanical shearing and high-pressure homogenization for nanoscale cellulose fibrils and strong gels. *Biomacromolecules* **2007**, *8*, 1934–1941. [CrossRef] [PubMed]
68. Spence, K.L.; Venditti, R.A.; Rojas, O.J.; Habibi, Y.; Pawlak, J.J. A comparative study of energy consumption and physical properties of microfibrillated cellulose produced by different processing methods. *Cellulose* **2011**, *18*, 1097–1111. [CrossRef]
69. Jonoobi, M.; Mathew, A.P.; Oksman, K. Producing low-cost cellulose nanofiber from sludge as new source of raw materials. *Ind. Crops Prod.* **2012**, *40*, 232–238. [CrossRef]

70. Josset, S.; Orsolini, P.; Siqueira, G.; Tejado, A.; Tingaut, P.; Zimmermann, T. Energy consumption of the nanofibrillation of bleached pulp, wheat straw and recycled newspaper through a grinding process. *Nord. Pulp Pap. Res. J.* **2014**, *29*, 167–175. [CrossRef]
71. Miao, C.; Hamad, W.Y. Cellulose reinforced polymer composites and nanocomposites: A critical review. *Cellulose* **2013**, *20*, 2221–2262. [CrossRef]
72. Siqueira, G.; Bras, J.; Dufresne, A. Cellulosic bionanocomposites: A review of preparation, properties and applications. *Polymers* **2010**, *2*, 728–765. [CrossRef]
73. Wågberg, L.; Decher, G.; Norgren, M.; Lindström, T.; Ankerfors, M.; Axnäs, K. The build-up of polyelectrolyte multilayers of microfibrillated cellulose and cationic polyelectrolytes. *Langmuir* **2008**, *24*, 784–795. [CrossRef]
74. Naderi, A.; Lindström, T.; Sundström, J. Repeated homogenization, a route for decreasing the energy consumption in the manufacturing process of carboxymethylated nanofibrillated cellulose? *Cellulose* **2015**, *22*, 1147–1157. [CrossRef]
75. Missoum, K.; Belgacem, M.N.; Bras, J. Nanofibrillated cellulose surface modification: A review. *Materials* **2013**, *6*, 1745–1766. [CrossRef] [PubMed]
76. Rol, F.; Belgacem, M.N.; Gandini, A.; Bras, J. Recent advances in surface-modified cellulose nanofibrils. *Prog. Polym. Sci.* **2019**, *88*, 241–264. [CrossRef]
77. Jursic, B.S.; Zdravkovski, Z. A Simple Preparation of Amides from Acids and Amines by Heating of Their Mixture. *Synth. Commun.* **1993**, *23*, 2761–2770. [CrossRef]
78. Brochier Salon, M.-C.; Gerbaud, G.; Abdelmouleh, M.; Bruzzese, C.; Boufi, S.; Belgacem, M.N. Studies of interactions between silane coupling agents and cellulose fibers with liquid and solid-state NMR. *Magn. Reson. Chem.* **2007**, *45*, 473–483. [CrossRef]
79. Gebald, C.; Wurzbacher, J.A.; Tingaut, P.; Zimmermann, T.; Steinfeld, A. Amine-Based Nanofibrillated Cellulose as Adsorbent for CO_2 Capture from Air. *Environ. Sci. Technol.* **2011**, *45*, 9101–9108. [CrossRef]
80. Missoum, K.; Belgacem, M.N.; Barnes, J.-P.; Brochier-Salon, M.-C.; Bras, J. Nanofibrillated cellulose surface grafting in ionic liquid. *Soft Matter* **2012**, *8*, 8338–8349. [CrossRef]
81. Lavoine, N.; Bras, J.; Saito, T.; Isogai, A. Improvement of the Thermal Stability of TEMPO-Oxidized Cellulose Nanofi brils by Heat-Induced Conversion of Ionic Bonds to Amide Bonds. *Macromol. Rapid Commun.* **2016**, *37*, 1033–1039. [CrossRef]
82. Brochier Salon, M.-C.; Belgacem, M.N. Competition between hydrolysis and condensation reactions of trialkoxysilanes, as a function of the amount of water and the nature of the organic group. *Colloids Surf. A Physicochem. Eng. Asp.* **2010**, *366*, 147–154. [CrossRef]
83. Brochier Salon, M.-C.; Belgacem, M. N, Hydrolysis-condensation kinetics of different silane coupling agents, Phosphorus. *Sulfur Silicon* **2011**, *186*, 240–254. [CrossRef]
84. Beari, F.; Brand, M.; Jenkner, P.; Lehnert, R.; Metternich, H.; Monkiewicz, J.; Siesler, H. Organofunctional alkoxysilanes in dilute aqueous solution: New accounts on the dynamic structural mutability. *J. Organomet. Chem.* **2001**, *625*, 208–216. [CrossRef]
85. Liao, J.W.; Wang, Z.; Gao, C.; Wang, M.; Yan, K.; Xie, X.; Zhao, S.; Wang, J.; Wang, S. A high performance PVAm–HT membrane containing high-speed facilitated transport channels for CO_2 separation. *J. Mater. Chem. A* **2015**, *3*, 16746–16761. [CrossRef]
86. Labet, M.T.; Thielemans, W.; Dufresne, A. Polymer Grafting onto Starch Nanocrystals. *Biomacromolecules* **2007**, *8*, 2916–2927. [CrossRef] [PubMed]